Tracer-encapsulated solid pellet injection system

メタデータ	言語: eng
	出版者:
	公開日: 2012-09-11
	キーワード (Ja):
	キーワード (En):
	作成者: Sudo, Shigeru, Tamura, Naoki
	メールアドレス:
	所属:
URL	http://hdl.handle.net/10655/8930

Tracer-encapsulated solid pellet injection system

Shigeru Sudo and Naoki Tamura

Related Articles

Sub-ppt gas detection with pristine graphene
Appl. Phys. Lett. 101, 053119 (2012)

Temporally resolved plasma composition measurements by collective Thomson scattering in TEXTOR (invited)
Rev. Sci. Instrum. 83, 10E307 (2012)

Accumulation mode field-effect transistors for improved sensitivity in nanowire-based biosensors
Appl. Phys. Lett. 100, 213703 (2012)

The evolution of solid density within a thermal explosion. I. Proton radiography of pre-ignition expansion, material motion, and chemical decomposition
J. Appl. Phys. 111, 103515 (2012)

Surface oxide on thin films of yttrium hydride studied by neutron reflectometry
Appl. Phys. Lett. 100, 191604 (2012)

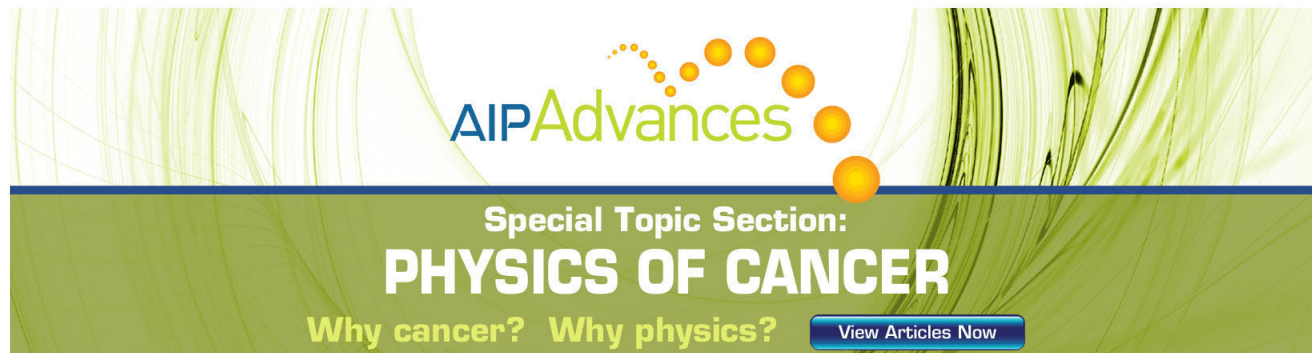## Additional information on Rev. Sci. Instrum.

Journal Homepage: http://rsi.aip.org

Journal Information: http://rsi.aip.org/about/about_the_journal

Top downloads: http://rsi.aip.org/features/most_downloaded

Information for Authors: http://rsi.aip.org/authors

Tracer-encapsulated solid pellet injection system

Shigeru Sudo[a)] and Naoki Tamura

National Institute for Fusion Science, National Institutes of Natural Sciences, 322-6 Oroshi-Cho, Toki, Gifu 509-5292, Japan

The method of tracer-encapsulated solid pellet (TESPEL) is now flourishing in various fields. The original purpose to study impurity transport without giving substantial perturbation on the plasma is implemented successfully for years. In addition to this, TESPEL is being intensively applied to study thermal (especially non-local) transport, high energy particles with the use of TESPEL ablation cloud, and spectroscopy from the viewpoint of atomic data. It is now further growing up to the utilization of multiple tracer methods which was not planned at the initial phase of the project. The proof-of-principle experiment using triple tracers has been successfully implemented. This opens a way to compare the Z dependence or mass dependence of impurity transport. In this article, as TESPEL is used in a variety of fields, the TESPEL injection system is summarized together with the method of TESPEL production, TESPEL storage disk, TESPEL guide system, and the differential pumping system. Also, the observation system for TESPEL flight and TESPEL ablation is explained. © 2012 American Institute of Physics. [doi:10.1063/1.3681447]

I. INTRODUCTION

So far, various researches on pellet fuelling and diagnostic applications of hydrogen and impurity pellet injection in tokamaks and helical systems have been done as described in some reviews.[1–4] In order to diagnose particle transport more accurately than the case with a simple impurity pellet injection, we have developed a method using a tracer-encapsulated solid pellet (TESPEL).[5–9] TESPEL consists of polystyrene (polymer: $-CH(C_6H_5)CH_2-$) as an outer part, and some tracers which are not intrinsic components in the plasma as the core part of TESPEL. The concept of the TESPEL configuration is shown in Fig. 1. The schematic view of the whole TESPEL diagnostic system is shown in Fig. 2. The essential feature of this method is based upon the production of both a poloidally and toroidally localized particle sources as tracers, which are deposited at first in a very small volume (of the order of 1 cm^3) in the plasma in contrast to conventional methods, such as impurity pellet injection and laser blow-off methods. Thus, the radial localization of the tracers on a certain annular magnetic surface can be realized, which gives advantage for impurity transport study. After injection of such a TESPEL into a plasma, the locally deposited "tracer" particles (originating from the core of TESPEL) will be immediately ionized and heated by the bulk electrons and ions. These tracer particles move along magnetic field lines at first, and then they fill the magnetic surface and diffuse radially outward (or inward by pinch effect in some cases). Such motion of the tracer particles may be detected with spectroscopic methods such as characteristic line emission in the range from ultraviolet to soft x-ray and also a charge exchange recombination spectroscopy with spatial resolution at the location of the neutral beam. Thus, an accurate measurement of particle transport in the plasma becomes possible owing to the localized deposition of the tracer particles, and

new significant information about transport characteristics will be obtained. Furthermore, with this method, the amount of the deposited particles in the plasma can be precisely identified because of the known amount of the tracer particles put in the core of TESPEL. The TESPEL injection system has been working reliably, and owing to the flexibility such as TESPEL shell size selection and wide selection of tracer material, TESPEL is being now utilized for the multiple purposes.[5] These are investigations about impurity transport, heat transport, high energy particles, and spectroscopic study from the viewpoint of atomic data. In this article, the whole TESPEL injection system is described together with the method of TESPEL production, TESPEL storage disk, TESPEL guide system, and the differential pumping system.

II. TESPEL PRODUCTION AND STORAGE

The outer shell of TESPEL consists of polystyrene as stated above. The technology of the polystyrene ball production has been well established,[10] which has been mainly developed for usage of target pellet in the laser fusion experiments. The typical diameter ranges 0.2–7 mm, and the high quality shell formation with various wall thickness (typically 5–150 μm) is also available with a density-matched emulsion method.

To form a TESPEL, the tracer particles should be put inside of the polystyrene ball or shell. The shell size should be chosen according to the following requirements:

1. Amount of electrons in the ball or shell should be low enough so that the increase of the electron density after the pellet injection does not disturb the target plasma much;
2. The ball or shell thickness should provide desired location of the deposited core atoms under given background plasma conditions such as electron temperature as a main player of pellet ablation;

[a)] Electronic mail: sudo@nifs.ac.jp.

FIG. 1. Schematic view of configuration of TESPEL.

3 The pellet size should be large enough for handling with a standard technology and also for the appropriate acceleration of the pellets.

For the purpose of injection to the large helical device (LHD),[11] the diameter of the ball or shells used for TESPEL production is typically in the range of 0.4–0.9 mm (recently larger size is also available). In case of the diameter of 0.5 mm, for example, the total amount of ions is 6.4×10^{18}, and the total amount of electrons to be deposited in the plasma (under the condition that all the particles in TESPEL are fully ionized) is 2.3×10^{19}. On the other hand, the total amount of electrons in the typical LHD plasma with the average electron density of 3×10^{19} m^{-3} is about 9×10^{20} electrons; thus, the ratio of the electron numbers from TESPEL to that of the LHD plasma is only 2.5%. Even under such condition, TESPEL can still penetrate into the location of ρ (=r/a) = 0.6–0.7 of the typical LHD plasma with Te = 3–4 keV in the core of the plasma. Considering the case of 5 titanium balls with diameter of 50 μm as tracer (typical amount for the standard experiment), the total amount of titanium ions in the TESPEL is 1.9×10^{16} particles, and the corresponding electron number is 4.1×10^{17}, when all the titanium ions are fully ionized. These numbers are much smaller than those of ions and electrons in the LHD plasma. So, the TESPEL concept is easily applicable for the ordinary conditions of the LHD plasmas (and also for the other magnetic confining devices such as helical systems and tokamaks). A standard TESPEL production method is described in Sec. II A.

FIG. 2. Schematic view of the whole TESPEL diagnostic system.

A. TESPEL production method

With utilizing a polystyrene ball or shell, we put tracer particles inside of the polystyrene ball or shell to form a TESPEL. The polystyrene ball of which size is relevant to our purpose, is now commercially available from a Japanese company (Hamamatsu Photonics K.K.). The key procedure of TESPEL production from starting such polystyrene balls is as follows:

1 Selecting the polystyrene ball with necessary size (which is confirmed with a microscope) and holding each ball on a glass plate with acrylic resin glue which can be dried up under UV light;

2 Making a hole in the selected ball with a micro drill (typical diameter is 200 μm, but it can be downsized to 50 μm diameter for the case of the required hole with diameter of 70–90 μm);

3 Inserting the tracer material (in forms of sphere, powder, or fragment status depending on the tracer material feature) of known amount of the quantity into the polystyrene ball;

4 Closing the hole with a small polystyrene ball (typical diameter is 200 μm according to the hole diameter) of which surface is partially dissolved by toluene as a role of glue and is rapidly dried up;

5 Separating the completed TESPEL from the solid glue on a glass plate; and

6 Putting each TESPEL in each hole of the TESPEL storage disk, and keeping TESPELs in the disk under the vacuum condition (it is necessary when the tracer is reactive material such as Li under air). The outer size, the species of tracer materials, and the amount of tracer materials of each TESPEL are registered according to the location of the hole of the TESPEL storage disk.

A typical TESPEL production procedure is shown in Fig. 3. The initial polystyrene ball is shown in Fig. 3(a), and the status of the drilled polystyrene ball is shown in Fig. 3(b). In Fig. 3(c), the status of the titanium balls as tracer particles installed inside the drilled polystyrene ball is shown (the step 3 of the above procedure), and the status of the completed TESPEL closed a hole with a lid (a small polystyrene ball) is shown in Fig. 3(d).

B. TESPEL storage disk

The completed TESPEL is stored in a TESPEL storage disk. The conceptual design of the TESPEL storage disk and the related components are shown in Fig. 4. The TESPEL storage disk is held with two housings from both sides. The total 60 holes in the TESPEL storage disk are located on the circumferences with diameter of 80 mm, and the holes are separated equally, thus the separation angle is 6°. Fifty nine TESPELs can be stored in the holes of the TESPEL storage disk made of stainless steel, while one empty hole is used for checking the precise matching of the hole position of the storage disk with the hole of the housing flange from outside. This procedure is important for reliable operation. For the case of the hole diameter of 1 mm, we check the matching
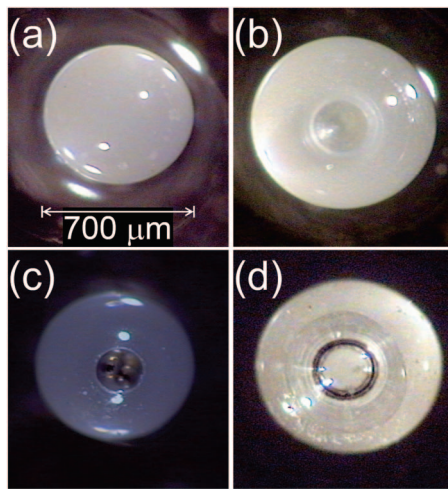
FIG. 3. (Color) TESPEL production procedure: (a) status of the initial polystyrene ball, (b) status of the drilled polystyrene ball, (c) status of the titanium tracer balls inside the drilled polystyrene ball, and (d) status of the completed TESPEL with the closed hole.

of the holes with passing a stainless steel wire of certain diameter through the holes. The diameter of the wire is changed until it can pass thorough both the holes. As one example of the testing data, the wire with diameter of 0.96 mm can go through two holes simultaneously for the 56 holes versus total 59 holes, and the wire with diameter of 0.94 mm can go through for the rest of three cases. This condition gives 100% reliability of TESPEL ejection for TESPEL with diameter of 0.4–0.9 mm. The TESPEL storage disk has a shaft in the center, and this shaft is connected to an ac servo motor. This motor is controlled with the feedback control system for remote control. The TESPEL storage disk is rotated with the motor. For smooth operation of the disk rotation, both the bearings A (shown in Fig. 4) between the storage disk and the housing and the bearings B (shown in Fig. 4) around the shaft are very important for precise positioning of the disk. Each TESPEL in each hole is registered as stated above so that TESPEL with the required tracer can be ejected by selecting the position number of TESPEL with remote control. Usually some TESPELs without tracer are also prepared for reference shot which proved very useful.
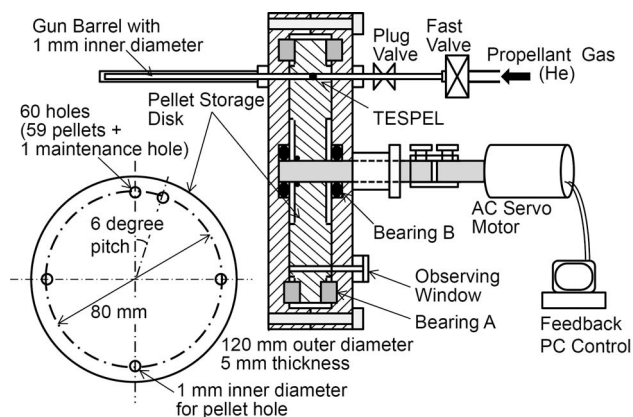
FIG. 4. TESPEL storage disk.
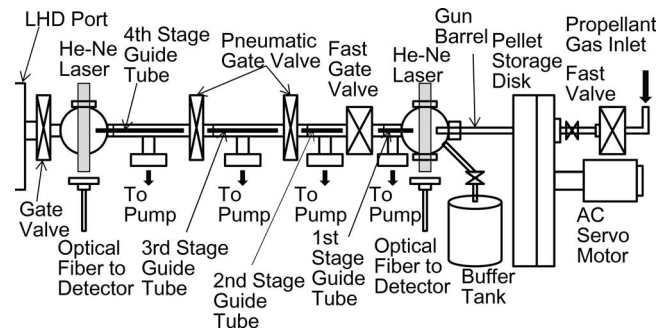
FIG. 5. TESPEL injection system with function of differential pumping.

III. TESPEL GUIDE TUBES AND DIFFERENTIAL PUMPING SYSTEM

The TESPEL is accelerated through the gun barrel (with the inner diameter of 1 mm and the length of 167 mm, shown in Fig. 4) by He gas with typical pressure of 1–3 MPa. The He gas is introduced by a fast valve with opening time of several ms. As a result, the TESPEL velocity ranges from 300 to 400 m/s. This is measured with the time of flight method as shown in Fig. 5. When TESPEL interrupts the He–Ne laser beam at two different locations, it is detected optically, and thus the velocity can be deduced. With using this signal as a trigger for the fast flash lamp, the shadow image of TESPEL can be also taken. Then, soundness (such as unbroken condition) of the TESPEL shape in flight can be confirmed. For preventing the high pressure He gas from getting into the LHD plasma, the differential pumping system is constructed. The TESPEL injection system with function of differential pumping is shown in Fig. 5. For differential pumping, 4 guide tubes and 4 gate valves are set. The 4 gate valves are closed immediately after TESPEL ejection to prevent the propellant He gas from getting into the LHD plasma. The residual propellant gas is pumped out by turbo-molecular pumps. The guide tubes made of bright-annealed (BA) stainless tubes have two functions. One is to guide TESPEL adequately to the LHD plasma and the other is to reduce the conductance of gas flow. Here, the dispersion of TESPEL flight angle should be taken into account to transfer TESPEL to the next guide tube. The testing shows that the dispersion of pellet ejection angle from the gun barrel is 1.6° for full angle. So, we designed the inner diameter of the guide tubes considering this dispersion of the angle and the interval between guide tubes which is a necessary space for locating a gate valve. Based on this, further we selected the guide tubes from the commercially available BA pipes. The length of the guide tubes is selected as long as possible within the practical availability for reducing the conductance of gas flow. Taking all these into consideration, the final design of the guide tubes is given in Table I where inner diameter, length of the guide tubes, and interval of the guide tubes are shown. The full angle calculated based on the interval and the inner diameter is also shown. Here, the interval between guide tubes in the column of the 1st guide tube means the space between the barrel outlet and the 1st tube inlet. The other column of the interval of the nth guide tube means the interval between the nth guide tube and the (n–1)th guide tube. All the

TABLE I. Guide tube dimensions.

Guide Tube	Outer diameter (mm)	Inner diameter (mm)	Length (mm)	d[a] (mm)	dθ[b] (degree)
1st	4.75	2.27	139	8[c]	4.5
2nd	6.0	4.0	1495.5	20.5	2.4
3rd	9.53	7.53	392	50	2.0
4th	12.7	10.7	2715	37	2.5

Dispersion of pellet ejection angle: 1.6°.
Material of tubes: BA tubes.
[a]Space between tubes.
[b]Designed angle between tubes.
[c]Between the barrel and 1st tube.

calculated angles are larger than the above dispersion angle of 1.6°, so TESPEL can be transferred appropriately. It is experimentally confirmed as almost 100% transferring rate.

IV. TESPEL INJECTION SCENARIO

Flow chart of TESPEL injection scenario including control and measurements is shown in Fig. 6. The system is fully remotely controlled. At first, we select the number of the TESPEL location from 1 to 59, all of which size and tracer material are registered beforehand as stated previously, and then push the button on the remote personal computer to start rotation of the TESPEL storage disk for setting up the required TESPEL at the ejection position approximately at t = −120 s (here, t = 0 s is defined as the triggering time of the high pressure fast valve to introduce the propellant helium gas). Then, the gate valves between guide tubes and the gate valve at the LHD port are opened several seconds before TESPEL injection. TESPEL injection timing is set beforehand at a certain delay from the LHD plasma discharge depending on the experimental plan. After the LHD plasma is started, the high pressure fast valve is triggered to introduce the propellant helium gas at t = 0 s, then TESPEL is ejected with velocity of typically 400 m/s, and it goes through the guide tubes, then

FIG. 6. Flow chart of TESPEL injection system.

reaches the plasma ∼15 ms after TESPEL ejection. The signal dip of the photo detector due to TESPEL shadow of the He–Ne laser beam triggers the pellet ablation diagnostics and other relevant measurement devices in addition to the pellet velocity measurement. After some short delay, the gate valves between guide tubes and the gate valve at the LHD port are closed for preventing the propellant gas from getting into the LHD vacuum chamber. The gate valve between the gun barrel and the 1st guide tube is closing in about 10 ms, and the gate valve between the 1st guide tube and the 2nd guide tube is closing in about 200 ms, while the operation of the other gate valves is standard; namely, closing time of 1–2 s. The function of the differential pumping system is experimentally confirmed, as the pressure increase is not detected within the accuracy of the monitor in the testing of injection into the LHD vacuum chamber without plasma. After closing gate valves, vacuum chambers are evacuated by turbo-molecular pumps. The standard interval of the LHD plasma discharge operation is 3 min, and the TESPEL injection cycle described here is achieved within this interval.

V. DIAGNOSTICS IN TESPEL INJECTION EXPERIMENTS

There are several groups of diagnostics in TESPEL injection experiments. First one is the pellet observation system. This includes the pellet velocity measurement by a time-of-flight method with two pairs of set of a He–Ne laser and a photo detector. And the pellet shadowgraph with a CCD camera illuminated by a fast flush lump (pulse duration of about 70 ns) is used to observe the pellet shape in flight.

The second group is to observe pellet ablation. With the optical system (lens, interference filters, and optical fibers) and photo detectors (photomultipliers), the ablation light from the TESPEL shell and tracer can be observed separately. So, we could identify the location of the tracer deposition inside the plasma with knowing the TESPEL velocity. This can be also confirmed by two CCD cameras observation with certain interference filters; one for the carbon of the TESPEL shell and the other for the tracer particles. Then, the time integrated 2D images (with video rate) of the emission light can be checked. We also utilized a spectrometer and a CCD camera with a high speed temporal resolution (about 50 μs) instead of the filter and the photomultiplier to get higher resolution of spectrum with temporal resolution. With this, for example, the spectral broadening of the H_β (Hydrogen Balmer β line) can be observed, which is due to the Stark broadening. Thus, the electron density of the ablation cloud can be deduced. This, however, is the spatially average data in the pellet ablation cloud. So, to get the two-dimensional density profile in the ablated cloud, the new system, called NIOS system, with 9 narrow bandwidth filters and fast CCD camera has been installed.[12] With this system, we have obtained the density and the electron temperature 2D profiles in the pellet vicinity.[13] The cloud electron temperature is estimated by the ratio of the full H_β intensity to continuum spectra intensity.

The third group is for the observation of the tracer behavior for studying impurity transport. The soft x-ray pulse height analyzer is appropriate to observe the characteristic x-ray
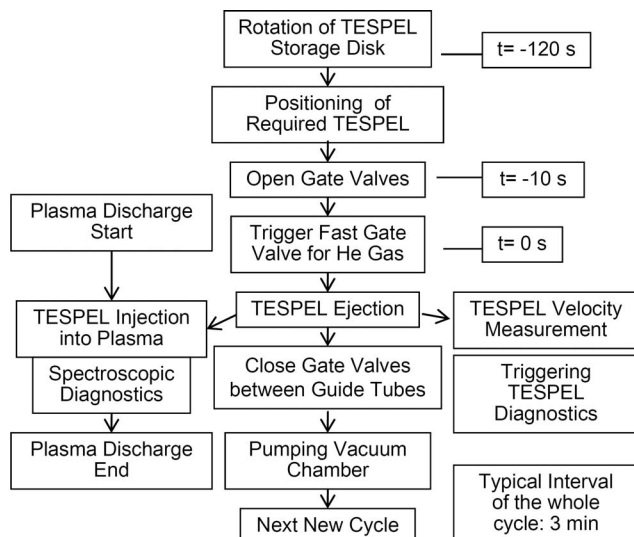
TABLE II. Tracer atoms used so far in the experiment.

Z	3	9	12	13	22	23	
Atom	Li	F	Mg	Al	Ti	V	
Compound	LiH	$(CF_2–CF_2)_n$					
Z	25	26	27	28	50	64	74
Atom	Mn	Fe	Co	Ni	Sn	Gd	W

Z = 3–13: Charge exchange recombination spectroscopy; Z = 22–28: Soft x-ray pulse height analysis, spectroscopy in the vacuum ultra violet regime; Z = 50–74: For studying spectroscopic data in the ultraviolet regime.

FIG. 7. The vacuum ultraviolet spectroscopic data before (t = 3.65 s) and after (t = 3.85 s) injection of a TESPEL with triple tracers: V, Mn, and Co. The intensity I (arbitrary unit) versus the wavelength (nm). The time resolution is 50 ms. The base of the spectra before TESPEL injection is shifted downward to avoid overlapping. The TESPEL is injected at t = 3.69 s. Li-like line emissions and also the other lines from these three tracers are clearly observed after TESPEL injection, while these are negligible before TESPEL injection. As Fe is an intrinsic impurity, the Fe line (Fe XXIV) intensity is unchanged before and after TESPEL injection.

line such as K_α line. The ultraviolet spectrometer is adequate mainly for the observation of the tracers in the plasma periphery. The charge exchange recombination spectroscopy is also useful for observing the emission light due to recombination induced after the charge exchange between the tracer (such as lithium) and the neutral beam.[14,15] Impurity transport in the magnetic island is also studied with TESPEL. Controlling the TESPEL size and appropriate shape and location of the magnetic island which can be controlled with the auxiliary coils, the tracer can be deposited inside the island. The impurity behavior can be observed by a multi-chord bolometric detector array.[16,17] Tracer atoms used so far in the LHD experiment are listed in Table II. As shown in the table, in case of low Z (3–13), the spectroscopy in the ultraviolet and visible regimes is adequate, and charge exchange recombination spectroscopy is appropriate because of larger cross section, and in case of medium Z (22–28), the spectroscopy in the ultraviolet and the soft x-ray regimes is adequate, and as for the latter, K_α line emission is available using pulse height analysis. In case of high Z (50–74), spectroscopic data in the ultraviolet regime are mainly interested for our present electron temperature level, although the different spectroscopic method will become more important in case of higher temperature. To study impurity transport, it is interesting to see the dependence of the charge Z of impurities under the same plasma condition. So far, we have replaced tracers in TESPEL shot by shot. To avoid ambiguity of the background plasma condition, we are developing the method of injecting a TESPEL with multiple tracers. Then, the plasma condition is just the same for the different tracers, and precise comparison between the different Z tracers becomes possible. As for the proof-of-principle experiment, we injected a TESPEL with triple tracers: V, Mn, and Co. The vacuum ultraviolet spectroscopic data (in the range of 15–27 nm) before (t = 3.65 s) and after (t = 3.85 s) injection of a TESPEL with these triple tracers is shown in Fig. 7. A Schwob-Fraenkel 2.0 m SOXMOS (Ref. 18) system with time resolution of 50 ms is used. The TESPEL is injected at t = 3.69 s. Li-like line emissions and also the other lines from these three tracers are clearly observed after TESPEL injection, while these are negligible before TESPEL injection. The base of the spectra before TESPEL injection is shifted downward to avoid overlapping of the lines. Lines of Fe as an intrinsic impurity are observed with a similar intensity both before and after TESPEL injection.

The fourth group is to utilize TESPEL injection for the other purposes. As TESPEL can be controlled quite well to deposit tracers in certain location in the plasma, it is very ap-
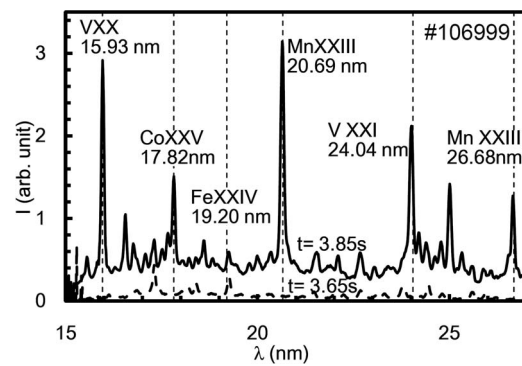
propriate to put any interested tracer under the certain electron temperature and density. So, this feature is utilized for studying atomic data such as spectroscopic data of EUV light, for example, from Sn (Refs. 19 and 20) useful for industrial application and Fe spectra useful for astronomy. As another application, the charge exchange between the TESPEL ablation cloud and the high energy particles in the plasma is utilized to neutralize the high energy ions. Then, the high energy neutral particles flowing away from the pellet ablation cloud can be detected outside of the plasma. Thus, high energy particle energy distribution and the pitch angle of the flight direction can be obtained.[21,22] Knowing the pellet path and having the temporal resolution, the location of the origin of the fast particles can be analyzed. For example, this method made clear that the intense production of high energy particles is located at the ion cyclotron resonance layer in case of ion cyclotron heating experiments.[23] One more application is to utilize TESPEL as a small perturbation to the plasma to observe the transient response of the plasma.[24–26] Owing to the flexibility that the TESPEL size can be relatively easily changed, the non-local heat transport has been well investigated. The small perturbation in the periphery of the plasma affects the core of the plasma much faster than the diffusion time. Under certain condition, the electron temperature (ion temperature also in some case) in the core increases very fast, while the electron temperature in the plasma periphery decreases due to plasma cooling by TESPEL injection.[27,28] This gives very good opportunity to investigate the heat transport feature.

ACKNOWLEDGMENTS

[1] S. K. Combs, Rev. Sci. Instrum. **64**, 1679 (1993).

[2] S. L. Milora, W. A. Houlberg, L. L. Lengyel, and V. Mertens, Nucl. Fusion **35**, 657 (1995).

[3] B. V. Kuteev, Tech. Phys. **44**, 1058 (1999).

[4] B. Pegourie, Plasma Phys. Controlled Fusion **49**, R87 (2007).

[5] S. Sudo, J. Plasma Fusion Res. **69**, 1349 (1993).

[6] K. V. Khlopenkov and S. Sudo, Rev. Sci. Instrum. **69**, 3196 (1998).

[7] S. Sudo, N. Tamura, K. Khlopenkov, S. Mutoh, H. Funaba, I. Viniar, V. Sergeev, K. Sato, K. Ida, K. Kawahata, A. Komori, K. Matsuoka, K. Narihara, S. Okamura, N. Ohyabu, K. Tanaka, and O. Motojima, Plasma Phys. Controlled Fusion **44**, 129 (2002).

[8] S. Sudo, T. Ozaki, N. Ashikawa, M. Emoto, M. Goto, Y. Hamada, K. Ida, T. Ido, H. Iguchi, S. Inagaki, M. Isobe, K. Kawahata, K. Khlopenkov, T. Kobuchi, Y. Liang, S. Masuzaki, T. Minami, S. Morita, S. Muto, Y. Nagayama, H. Nakanishi, K. Narihara, A. Nishizawa, S. Ohdachi, M. Osakabe, B. J. Peterson, S. Sakakibara, M. Sasao, K. Sato, M. Shoji, N. Tamura, K. Tanaka, K. Toi, T. Tokuzawa, K. Watanabe, T. Watanabe, I. Yamada, LHD Team, P. Goncharov, A. Ejiri, S. Okajima, A. Mase, S. Tsuji-Iio, T. Akiyama, J. F. Lyon, L. N. Vyacheslavov, and A. Sanin, Plasma Phys. Controlled Fusion **45**, 1127 (2003).

[9] S. Sudo, N. Tamura, D. Kalinina, I. Vinyar, K. Sato, E. Veshchev, P. R. Goncharov, T. Ozaki, S. Inagaki, H. Funaba, S. Mutoh, Y. Igitkhanov, L. Yi, B. Peterson, D. Stutman, M. Finkenthal, and LHD Experimental Group, J. Plasma Fusion Res. **2**, S1013 (2007).

[10] M. Takagi, T. Norimatsu, T. Yamanaka, and S. Nakai, J. Vac. Sci. Technol. A **9**, 2145 (1991).

[11] O. Motojima, H. Yamada, A. Komori, N. Ohyabu, K. Kawahata, O. Kaneko, S. Masuzaki, A. Ejiri, M. Emoto, H. Funaba, M. Goto, K. Ida, H. Idei, S. Inagaki, N. Inoue, S. Kado, S. Kubo, R. Kumazawa, T. Minami, J. Miyazawa, T. Morisaki, S. Morita, S. Murakami, S. Muto, T. Mutoh, Y. Nagayama, Y. Nakamura, H. Nakanishi, K. Narihara, K. Nishimura, N. Noda, T. Kobuchi, S. Ohdachi, Y. Oka, M. Osakabe, T. Ozaki, B. J. Peterson, A. Sagara, S. Sakakibara, R. Sakamoto, H. Sasao, M. Sasao, K. Sato, M. Sato, T. Seki, T. Shimozuma, M. Shoji, H. Suzuki, Y. Takeiri, K. Tanaka, K. Toi, T. Tokuzawa, K. Tsumori, K. Tsuzuki, I. Yamada, S. Yamaguchi, M. Yokoyama, K. Y. Watanabe, T. Watari, Y. Hamada, K. Matsuoka, K. Murai, K. Ohkubo, I. Ohtake, M. Okamoto, S. Satoh, T. Satow, S. Sudo, S. Tanahashi, K. Yamazaki, M. Fujiwara, and A. Iiyoshi, Phys. Plasmas **6**, 1843 (1999).

[12] N. Tamura, V. Yu. Sergeev, D. V. Kalinina, I. V. Miroshnikov, K. Sato, I. A. Sharov, O. A. Bakhareva, D. M. Ivanova, V. M. Timokhin, S. Sudo, and B. V. Kuteev, Rev. Sci. Instrum. **79**, 10F541 (2008).

[13] I. A. Sharov, I. V. Miroshnikov, N. Tamura, V. Yu. Sergeev, S. Sudo, and B. V. Kuteev, in *Proceedings of the 37th EPS Conference on Plasma Physics, Dublin, Ireland, 2010*, p. 5.131; also see http://ocs.ciemat.es/EPS2010PAP/pdf/P5.131.pdf.

[14] D. Kalinina, S. Sudo, N. Tamura, V. Yu. Sergeev, and LHD Experimental Group, J. Plasma Fusion Res. SERIES **6**, 634 (2004); also see http://www.jspf.or.jp/JPFRS/index_vol6-4.html.

[15] D. Kalinina, S. Sudo, D. Stutman, M. Finkenthal, N. Tamura, K. Sato, and A. Matsubara, J. Plasma Fusion Res. **80**, 545 (2004).

[16] N. Tamura, Y. Liu, N. Iwama, S. Sudo, K. V. Khlopenkov, A. Yu. Kostrioukov, B. J. Peterson, S. Inagaki, Y. Nagayama, K. Kawahata, T. Morisaki, K. Ida, N. Ohyabu, A. Komori, and LHD Experimental Group, J. Plasma Fusion Res. SERIES **8**, 975 (2009); also see http://www.jspf.or.jp/JPFRS/index_vol8-6.html.

[17] N. Tamura, S. Sudo, K. Khlopenkov, A. Kostrioukov, B. Peterson, S. Inagaki, Y. Nagayama, K. Kawahata, T. Morisaki, K. Ida, N. Ohyabu, H. Suzuki, A. Komori, and LHD experimental groups, J. Plasma Fusion Res. **78**, 837 (2002).

[18] J. L. Schwob, A. W. Wouters, S. Suckewer, and M. Finkenthal, Rev. Sci. Instrum. **58**, 1601 (1987).

[19] C. Suzuki, T. Kato, K. Sato, N. Tamura, D. Kato, S. Sudo, N. Yamamoto, H. Tanuma, S. Suda, G. O'Sullivan, and A. Sasaki, J. Phys.: Conf. Ser. **163**, 012019 (2009).

[20] C. Suzuki, T. Kato, H. A. Sakaue, D. Kato, K. Sato, N. Tamura, S. Sudo, N. Yamamoto, H. Tanuma, H. Ohashi, R. D'Arcy, and G. O'Sullivan, J. Phys. B **43**, 074027 (2010).

[21] T. Ozaki, P. Goncharov, E. Veshchev, S. Sudo, and N. Tamura, Plasma Fusion Res. **2**, S1072 (2007).

[22] T. Ozaki, P. Goncharov, E. Veshchev, N. Tamura, S. Sudo, T. Seki, H. Kasahara, Y. Takase, and T. Ohsako, Rev. Sci. Instrum. **79**, 10E518 (2008).

[23] T. Ozaki, P. R. Goncharov, E. A. Veshchev N. Tamura, S. Sudo, T. Seki, and H. Kasahara, High Energy Particle Group, Wave Heating Group, and LHD Experimental Group, J. Plasma Fusion Res. SERIES **8**, 1089 (2009); also see http://www.jspf.or.jp/JPFRS/index_vol8-7.html.

[24] N. Tamura, K. Khlopenkov, V. Sergeev, B. Kuteev, S. Sudo, S. Muto, K. Sato, H. Funaba, S. Inagaki, Y. Nagayama, K. Kawahata, and LHD experimental group, J. Plasma Fusion Res. SERIES **5**, 400 (2002); also see http://www.jspf.or.jp/JPFRS/index_vol5-3.html.

[25] S. Inagaki, Y. Nagayama, K. Kawahata, N. Tamura, A. Yu. Kostrioukov, B. J. Peterson, S. Sudo, and LHD Experimental Group, J. Plasma Fusion Res. SERIES **5**, 409 (2002); also see http://www.jspf.or.jp/JPFRS/index_vol5-4.html.

[26] N. Tamura, S. Inagaki, K. Tanaka, C. Michael, T. Tokuzawa, T. Shimozuma, S. Kubo, R. Sakamoto, K. Ida, K. Itoh, D. Kalinina, S. Sudo, Y. Nagayama, K. Kawahata, A. Komori, and LHD experimental group, Nucl. Fusion **47**, 449 (2007).

[27] N. Tamura, K. Ida, S. Inagaki, K. Tanaka, T. Tokuzawa, K. Itoh, T. Shimozuma, S. Kubo, H. Tsuchiya, Y. Nagayama, K. Kawahata, S. Sudo, H. Yamada, and LHD Experiment Group, Contrib. Plasma Phys. **50**, 514 (2010).

[28] N. Tamura, S. Inagaki, T. Tokuzawa, C. Michael, K. Tanaka, K. Ida, T. Shimozuma, S. Kubo, K. Itoh, Y. Nagayama, K. Kawahata, S. Sudo, A. Komori, and LHD Experiment Group, Fusion Sci. Technol. **58**, 122 (2010); also see http://epubs.ans.org/?a=10799.